Available online at www.sciencedirect.com
ScienceDirect
Journal of the European Ceramic Society 30 (2010) 2699–2705
www.elsevier.com/locate/jeurceramsoc

Pressureless densification and mechanical properties of hafnium diboride doped with B_4C: From solid state sintering to liquid phase sintering

Ji Zou [a,b], Guo-Jun Zhang [a,*], Yan-Mei Kan [a]

[a] State Key Laboratory of High Performance Ceramics and Superfine Microstructures, Shanghai Institute of Ceramics, Shanghai 200050, China
[b] Graduate School of the Chinese Academy of Sciences, Beijing 100049, China

Received 15 December 2009; received in revised form 13 April 2010; accepted 23 April 2010
Available online 2 June 2010

Abstract

A pressureless sintering process, using a small amount of boron carbide (≤2 wt%) as sintering aid, was developed for the densification of hafnium diboride. Hafnium diboride ceramics with high relative density were obtained when the sintering temperature changed from 2100 °C to 2350 °C. However, the sintering mechanism was varied from solid state sintering (SSS, below 2300 °C) to liquid phase sintering (LPS, above 2300 °C). Boron carbide addition improved densification by removing the oxide impurities during solid state sintering and by forming a liquid phase which was well wetting hafnium diboride grains during liquid phase sintering process. The different roles of B_4C on the microstructure development and mechanical properties of the sintered ceramics were investigated.

Keywords: HfB_2; Pressureless sintering; Mechanical property; Solid state sintering; Liquid phase sintering

1. Introduction

Compared with the other IVB group transition metal diborides which belong to ultra-high temperature ceramics (UHTCs), hafnium diboride (HfB_2) has the highest melting point (3380 °C) and thermal conductivity (104 W m K^{-1}).[1,2] What is more, it owns moderate bending strength (300–500 MPa),[2–5] high hardness (20–28 GPa)[2–6] and relatively low coefficient of thermal expansion (6.3×10^{-6} K^{-1}).[2] The combinations of these properties make HfB_2 attractive for aerospace applications, especially for the sharp wing leading edges and rocket nozzles which can be operated up to 2400 °C for a short lifetime, or re-usable hot structures and missile launchers which can be used in the range of room temperature to 2000 °C for a long lifetime.[1,7]

Though emerging attentions on HfB_2 have been driven by the above applications, resulting from the strong covalent bonding and low self-diffusion coefficient of boride, the densification of HfB_2 can only be accomplished by hot pressing at 1790–1900 °C with applied pressure between 800 MPa and 1500 MPa.[3]

Hot pressing is very effective for the densification of UHTCs, however, pressureless sintering is more convenient and allows fabricating components to near-net shape. The breakthrough on pressureless sintering of transition metal diborides has been realized in recent years by adding the following kinds of sintering aids.

(i) Carbon containing additives such as C,[8,9] B_4C,[8,10,11] WC,[12,13] VC[14,15] or their mixtures.[8,16] These sintering aids can activate the raw powders by removing the oxide layers on the surface of transition borides. The adverse effect of oxygen contamination (in terms of B_2O_3, TiO_2, ZrO_2 or HfO_2 on the surface of the raw powders) on the densification of TiB_2, ZrB_2 or HfB_2 ceramics has been well illustrated.[5,8,11,17] Benefiting from the reactions between these additives and corresponding metal oxides, nearly fully dense ZrB_2[8–12] and HfB_2[5] have been sintered at the temperature range from 1850 °C to 2200 °C without external pressure.
(ii) Transition metals (Fe, Cr[18] and Ni[19]) and refractory metal silicides ($MoSi_2$,[4,20] $TiSi_2$[6] and $HfSi_2$[10]). These metals can form liquid phase during sintering process. Furthermore, these liquid phase formers can fill voids among matrix grains, favor the matter transport, and then accelerate the

* Corresponding author. Tel.: +86 21 52411080; fax: +86 21 52413122.
E-mail address: gjzhang@mail.sic.ac.cn (G.-J. Zhang).

0955-2219/$ – see front matter © 2010 Elsevier Ltd. All rights reserved.
doi:10.1016/j.jeurceramsoc.2010.04.033

densification process. Pressureless densification of ZrB_2 and HfB_2 also has been realized at 1900–1950 °C by adding a small amount of $MoSi_2$ (5–20 vol%).[4,20] Though no direct evidence on whether liquid phase exists in the sintering process of ZrB_2–$MoSi_2$ composites, Mizuguchi found Mo and Si were incorporated into ZrB_2 grain boundaries during sintering.[21]

Among the numerous sintering aids, B_4C is more suitable to be selected as the sintering aid.[8,10,11] The process of removing surface oxides by utilizing B_4C could be described as reaction (1).

$$7MO_2(cr) + 5B_4C(cr) \rightarrow 7MB_2(cr) + 3B_2O_3(l, g) + 5CO(g), \quad M = Ti, Zr and Hf \tag{1}$$

The preferential advantage for using B_4C as sintering aid is that the major reaction product in condense state by reaction (1) is MB_2 itself, which might result in an improved mechanical properties of MB_2 at elevated temperatures. Based on this characteristic, numerous results assessing the additional effect of B_4C on the sintering behavior and mechanical properties of ZrB_2[8,10,11] and HfB_2[5] have been explored.

Most of the investigations on the densification of ZrB_2 and HfB_2 were conducted below 2200 °C and believed that solid state sintering is the main sintering mechanism when using B_4C as sintering aid. However, liquid will form in the HfB_2–B_4C binary system at about 2330 °C,[22] a different role of B_4C must be played at such a high temperature from the viewpoint of kinetics. So the objective of the present study is to understand the different roles of B_4C on the sintering behavior and microstructure tailoring of HfB_2 by pressureless sintering. In addition, the mechanical properties of the as-sintered HfB_2 ceramics were also characterized and discussed.

2. Experimental procedure

HfB_2 powder (average particle size is 1.5 μm, purity > 99%, O: 0.15 wt%, C: 0.04 wt%, synthesized at 1600 °C using HfO_2 and B_4C as reactants[23]) and B_4C (D_{50} = 1.5 μm, the ratio of B and C was 3.7, Jingangzuan Boron Carbide Co. Ltd., Mudanjiang, China) were used as the starting materials. 0, 1, 2 wt% B_4C were added into HfB_2, and the corresponding powders were marked as HfB_2, HfB_2–1 wt% B_4C and HfB_2–2 wt% B_4C, respectively. The powder mixtures were ball-mixed for 12 h in acetone using Si_3N_4 balls, dried in a rotating evaporator and sieved through a mesh screen (−200 mesh).

The powder mixtures were uniaxially pressed at 30 MPa into rectangle pellets with dimensions of 37 mm × 30 mm × 5 mm and then compacted by cold isostatic pressing at 300 MPa. Sintering was conducted in a high temperature graphite resistant furnace (MRF3338, Materials Research Furnaces Inc., Suncook, USA). The compacts were sintered in vacuum from room temperature to 2000 °C, and continually heated to 2100 °C, 2150 °C, 2200 °C, 2300 °C and 2350 °C in argon atmosphere. In addition to the last dwelling at the desired sintering temperatures for 2 h, the total heating schedule also included another two isothermal holds at 1650 °C and 2000 °C for 0.5 h, respectively. The reasons that the two pre-sintering procedures were adopted and the details of the sintering program have been reported elsewhere.[5]

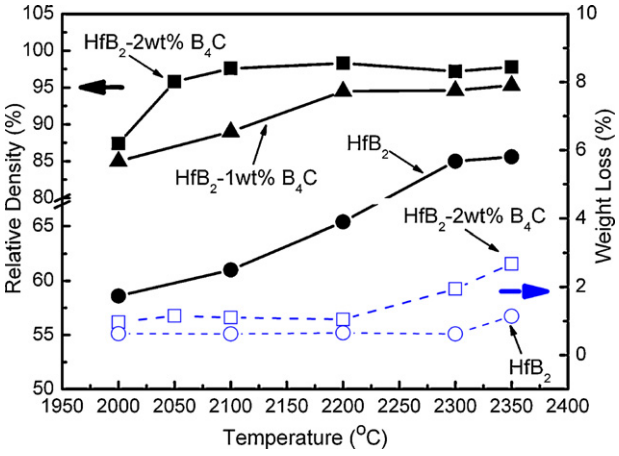

Fig. 1. Relative density and weight loss of HfB_2 with or without B_4C addition as a function of sintering temperature.

The bulk density of the sintered specimens was measured by the Archimedes method. The theoretical densities of the samples with B_4C additions were calculated based on that all the HfO_2 impurities have been consumed by B_4C. Some of the sintered samples were surface ground, polished, and thermal etched (1700–1800 °C in argon atmosphere) for scanning electron microscopy (SEM, JXA-8100, JEOL, Japan) analysis. The HfB_2 grain size and the dihedral angle (Φ) between HfB_2 grains and the liquid phase were quantified with an average of 100 areas using image analysis software. Vickers' hardness and fracture toughness were measured by the indentation method on the polished surfaces with a load of 1 kg and a dwell time of 10 s. The fracture toughness was calculated by Antis' equation. Young's modulus was tested by impulse excitation method. Flexural strength was measured by three-point bending on chamfered bars with dimensions of 2.5 mm × 2 mm × 25 mm. All the reported mechanical values were the average of five measurements.

3. Results and discussion

3.1. Densification behavior of HfB_2 doped with different amounts of B_4C

The relative density and weight loss of HfB_2 with or without B_4C as a function of sintering temperature are shown in Fig. 1 and the following issues could be drawn out:

(i) The densifications of pure HfB_2 just by elevating temperature were difficult. High dense HfB_2 ceramics could not be obtained even sintered at 2350 °C. The density of HfB_2 ceramics sintered at 2350 °C for 2 h was only 85.6% TD.
(ii) B_4C was very effective on promoting the densification of HfB_2, for it could react and remove the surface oxide impurities on HfB_2 powders based on reaction (1).[5] Either increasing the B_4C content or elevating the sintering

temperature could accelerate the densification of HfB_2. HfB_2–2 wt% B_4C with 97.5% TD could be obtained when sintered at 2100 °C, which was about 100–250 °C higher than that required for ZrB_2,[8] resulting from the more pronounced refractoriness characteristic of HfB_2.

(iii) Mass loss of the pellets occurred after sintering. Two possible ways could result in the weight loss of the samples, one was the evaporation of boron oxide species from the surface of the HfB_2 particles, and the other one was the reduction of HfO_2 by B_4C. Because no above-mentioned reaction occurred in pure HfB_2, its weight loss was lower than that of HfB_2–2 wt% B_4C, which was 0.6 wt% and 1 wt%, respectively, at the sintering temperatures of 2000 °C and 2200 °C. When the sintering temperature reached 2300 °C, a relatively remarkable mass loss in HfB_2–2 wt% B_4C (2 wt%) was measured, indicating that besides B_2O_3, other volatile phases appeared at this temperature. However, the same phenomenon did not occur in pure HfB_2.

3.2. Microstructures of the as-sintered HfB_2–2 wt% B_4C ceramics

HfB_2 with 2 wt% B_4C addition has the best sinterability, so its microstructure evolution combining with different sintering temperatures was investigated as shown in Fig. 2. Only limited apparent pores could be seen from these pictures, showing a good agreement with the measured high relative densities. Some B_4C grains are still left in Fig. 2a–e, because there was not enough HfO_2 to consume all of them. The grain size distributions of HfB_2 sintered at different temperatures are shown in Fig. 3. A mild grain growth of HfB_2 with narrow grain size distribution was observed in the temperature range of 2100–2200 °C. The grain growth behavior appears to be rapid at 2300 °C, and quasi-spherical HfB_2 grains with large size (60–120 μm) appeared, and some of the remaining pores were entrapped into these large grains (Fig. 2d). These microstructural features did not change remarkably when continuously elevating the sintering temperature to 2350 °C (Fig. 2e).

On the other hand, the morphologies of B_4C grains were much different at different sintering temperatures. When the pellets were sintered at 2100 °C, isolated B_4C grains with diameter of 2–3 μm were uniformly distributed in the HfB_2 matrix. Some B_4C particles (as arrowed in Fig. 2c) were entrapped into HfB_2 grains to form an intragranular type as the temperature reached 2200 °C. Though no apparent density change was measured with elevating the sintering temperature to 2300 °C or above, B_4C containing phases were changed to locate at the triangle pockets of HfB_2 grains (Fig. 2f). Such phenomenon should be a typical evidence for a liquid assistant sintering process.

3.3. Mechanical properties

The mechanical properties of some selected sintered HfB_2 ceramics are summarized in Table 1. The hardness varies from 17.0 GPa to 20.1 GPa, normally decreased with the increase of the grain size, which was in accordance with the Hall–Petch equation. However, the maximum hardness was still lower than the value of single-crystal HfB_2 (28 GPa). It could not be explained by the addition of B_4C, for B_4C having a higher hardness of 35 GPa.[24] Such phenomena have also been reported in PLS sintered ZrB_2 based composites.[4,12] However, the hardness deviations between ZrB_2 crystal (22 GPa) and ceramics (17 GPa) were less than that in HfB_2 system. The decreased hardness of ZrB_2 was regard as the microcracks formation in the interfaces between B_4C and ZrB_2 grains during the cooling process,[25] due to their thermal expansion coefficient (CTE) mismatch. The average CTE of HfB_2, ZrB_2 and B_4C was $6.3 \times 10^{-6}\,K^{-1}$, $5.9 \times 10^{-6}\,K^{-1}$ and $5.5 \times 10^{-6}\,K^{-1}$, respectively, thus the calculated residual stresses between B_4C and HfB_2 was 1.7 times larger than that between ZrB_2 and B_4C based on the Selsing's model.[26] It may be the reason for the more obviously hardness decrease in HfB_2–B_4C ceramics.

The Young's modulus (E) of the sintered HfB_2, varied from 526 GPa to 532 GPa, was not affected by its grain sizes and sintering temperatures. However, the values were higher than that reported in the literature (440–510 GPa),[2] for the high relative density of HfB_2 in the present work. E was very sensitive to the porosity, the decrease in relative density will result in the loss of elastic constant.

In contrast to the Young's modulus, which is an inherent property of the sample, the strength of the ceramics is determined by the critical defects. In case no larger defects could be identified, the critical flaw size is associated with the characteristic grain size of the sample. The average strength of HfB_2 sintered at 2100 °C, 2150 °C and 2200 °C was 483 MPa, 492 MPa and 469 MPa, no apparent trend related to their grain size was observed. It indicated that the critical defects (in terms of voids and cracks) in these samples were larger than the scale of grain size. The mentioned defects maybe resulted from the agglomerates during the forming stage or the sample machining process. A rapid strength decrease (to 191 MPa) was observed when HfB_2–2 wt% B_4C was sintered at 2300 °C, for the abnormal grain growth shown in Figs. 2d and 3d. Similar tendency occurred in fracture toughness results (Table 1).

3.4. The role of B_4C during the whole sintering process

The surface energy (γ_{SV}) of a powder compact is higher than the grain boundary energy (γ_{GB}) in a polycrystalline sintered body, so the reduction of the interfacial energy could occur from the view of thermodynamics and this is the driving force for a sintering process.[27] The driving force could be evaluated by the ratio of γ_{GB} and γ_{SV}. The higher γ_{SV}/γ_{GB}, the larger driving force could be obtained. According to this rule, any approach that can increase γ_{SV} or decrease γ_{GB} should enhance the densification process, and this principle was also applicable in the current study.

3.4.1. The increase of γ_{SV} when the sintering temperature was below 2300 °C

Oxygen contamination of non-oxide ceramic powders is usually caused by the surface oxidation during grinding or milling process. It has adverse effect on the sintering properties, for it can decrease the γ_{SV} of the corresponding powders. The reduction

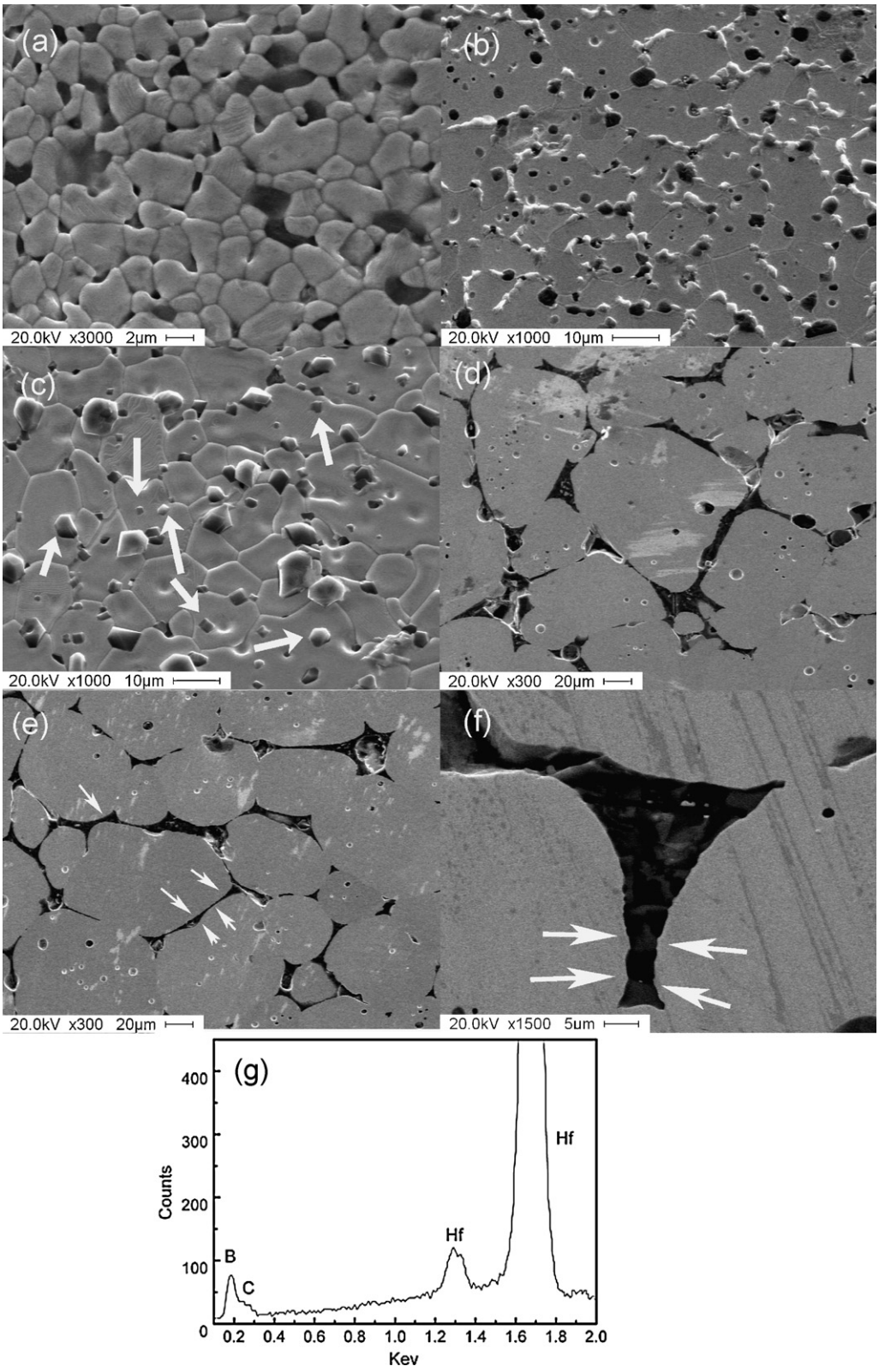

Fig. 2. Microstructures of HfB_2 pressureless sintered at (a) 2100 °C, (b) 2150 °C, (c) 2200 °C, (d) 2300 °C, (e and f) 2350 °C with 2 wt% B_4C additions. (g) EDS pattern of the black phase in Fig. 2f.

Table 1
Summary of the mechanical properties of HfB_2–2 wt% B_4C ceramics pressureless sintered at different temperatures.

Sintering temperature (°C)	Average grain size for HfB_2 (μm)	Young's modulus (GPa)	Hardness (GPa) Hv1	Strength (MPa)	Fracture toughness (MPa $m^{1/2}$)
2100	3.4	526	18.6 ± 1.1	483 ± 41	3.3 ± 0.2
2150	12.9	532	20.1 ± 2.1	492 ± 27	3.2 ± 0.1
2200	15.7	529	19.5 ± 1.2	469 ± 13	4.1 ± 0.4
2300	86.2	524	17.4 ± 1.7	191 ± 35	1.6 ± 0.4
2350	89.6	527	17.0 ± 0.6	/	1.7 ± 0.4

reaction between B_4C and HfO_2 was favorable when temperature was higher than 1400 °C, so the enhanced densification in the present work should be attributed to the increased γ_{SV} by the in situ purified surfaces of HfB_2 powders.

Based on reaction (1) and the oxygen content (0.7 wt%) in the as-mixed powders, 1 wt% B_4C was enough to remove the surface oxide impurities from the milled powder. However, an incomplete densification of HfB_2 was found (Fig. 1). This maybe caused by the restricted reduction ability of isolated B_4C grains surrounded by the limited HfB_2 grains (Fig. 2c). The efficiency to remove the oxygen contamination by B_4C was improved with the increase of its doping amount, due to the greater contact probability between B_4C and HfO_2 on the surfaces of HfB_2 powders.

The average grain size of HfB_2 was 12.9 μm and 15.7 μm when it was sintered at 2150 °C and 2200 °C, respectively (shown in Fig. 3). A relatively mild grain growth behavior was found in this temperature range. It indicated that solid state sintering mechanisms, such as grain boundary diffusion, were dominant in the densification process.[8] What is more, based on the above analysis, HfB_2–B_4C systems demonstrated a wide sintering temperature range of over 100 °C in solid state densification process, indicating a convenient temperature control in the solid state sintering process.

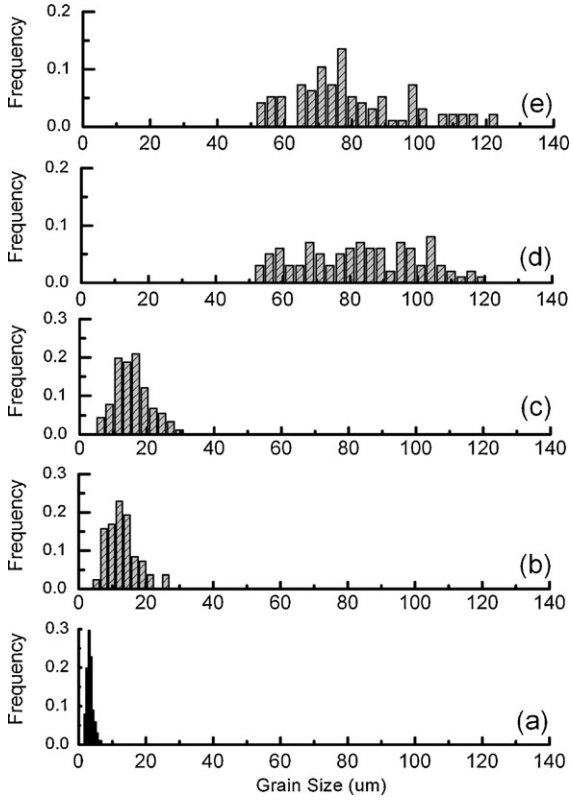

Fig. 3. Distribution of observed grain sizes on the polished and thermal etched section of HfB_2–2 wt% B_4C at different sintering temperatures: (a) 2100 °C, (b) 2150 °C, (c) 2200 °C, (d) 2300 °C and (e) 2350 °C.

3.4.2. *The decrease of γ_{GB} when the sintering temperature was above 2300 °C*

The partial Hf–C–B ternary phase diagram is shown in Fig. 4. The eutectic temperature in the HfB_2–B_4C system is 2330 ± 25 °C[22] and the compositions of the eutectic point are 78 mol% B_4C and 22 mol% HfB_2, respectively. However, considering a non-stoichiometric B_4C powder used in this work, the eutectic point changed from e3 to E2 (2260 °C) in the HfB_2–B_4C–C system.[22] The current sintering temperature was higher than 2260 °C, so liquid phase was formed by the reaction (2) between HfB_2 and B_4C. In equilibrium state, all the B_4C was consumed and converted to the liquid phase when the reaction

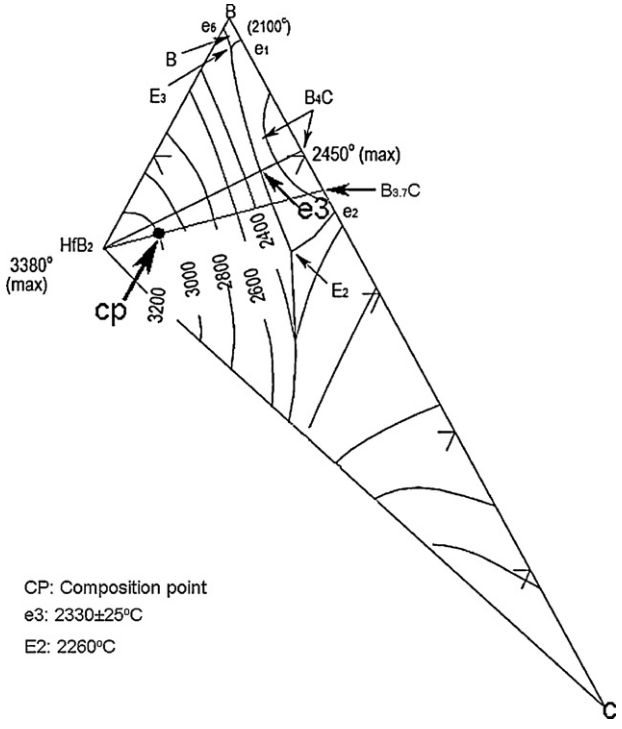

Fig. 4. Portion of the Hf–B–C ternary phase diagram.[22]

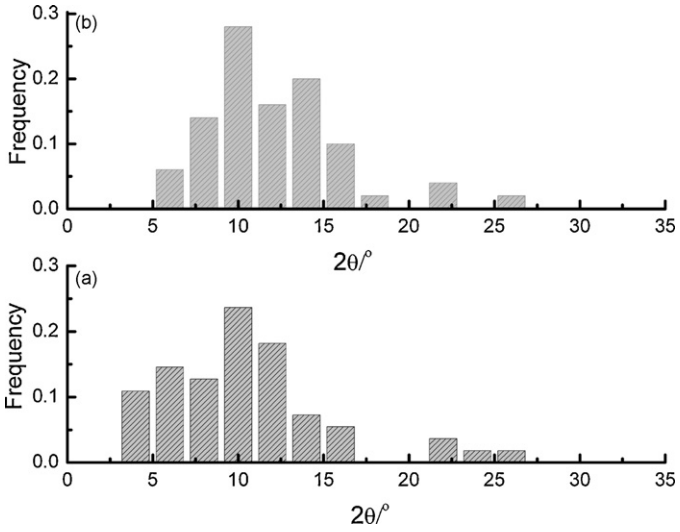

Fig. 5. Distribution of observed dihedral angles on the polished surface of HfB_2–2 wt% B_4C: (a) sintered at 2350 °C, (b) sintered at 2300 °C.

(3) completed.

$$HfB_2 + B_4C \rightarrow L + HfB_2 + B_4C \quad (2)$$

$$HfB_2 + B_4C \rightarrow L' + HfB_2 \quad (3)$$

The volatilization of the liquid phase during high temperature heat treatment process (2300–2350 °C for 2 h) can induce the weight loss of the samples as shown in Fig. 1. Its existence was also confirmed by a residual intergranular thin film between adjacent HfB_2 grains as arrowed in Fig. 2e and f. Such kind of liquid phase is effective on enhancing the densification process, for the surface of HfB_2 grains were totally wetting by it. EDS analysis of the liquid phase (Fig. 2g) indicated the existence of B, C, Hf and a slight amount of impurities. The measured average dihedral angle (Φ) between HfB_2 grains and the liquid phase was 11.1° when sintered at 2300 °C, slightly higher than that sintered at 2350 °C (9.5°). The relationship between interfacial energies (γ_{SS}), surface energies (γ_{SL}) and Φ could be determined by reaction (4).

$$\cos\left(\frac{\Phi}{2}\right) = 0.5\frac{\gamma_{SS}}{\gamma_{SL}} \quad (4)$$

γ_{SL} was considered as a function of temperature and decreased with the increase of temperature, thus resulted in the lower average dihedral angle in HfB_2–2 wt% B_4C sintered at 2350 °C when compared with that sintered at 2300 °C.

The calculated γ_{SS}/γ_{SL} was 1.99. It should be mentioned that it is just a rough estimation. γ_{SS} changed with different orientations of HfB_2 grains, thus a broad distribution of dihedral angle in the range from 2° to 26° was observed as shown in Fig. 5a and b.

Due to the strong covalent bonding character of HfB_2, its grain boundary energy should be relatively high. The effective role of the liquid phase is that it could decrease the γ_{GB} by wetting the grains with a thin layer of B–C film (arrowed in Fig. 2e) so as to increase the sintering driving force. On the other hand, the formed liquid can also accelerates the mass transfer via the dissolution–diffusion–precipitation process. The grains smaller than the average sized grain were dissolved and those larger than the average sized grain grow. The result of this process is the broad grain size distribution compared with the solid state sintering as shown in Fig. 3c and d.

4. Conclusions

Hafnium diboride ceramics were densified by pressureless sintering with B_4C as additives (≤2 wt%) at 2100–2350 °C for 2 h. Solid state sintering and liquid assistant sintering were observed and analyzed during the whole process and the following conclusions could be drawn:

1. The different roles of B_4C on the densification of HfB_2 during the whole sintering process. When the sintering temperature was below 2300 °C, B_4C would react with and remove the surface oxide impurities of HfB_2. The enhanced densification should be attributed to the submicron, surface cleaned HfB_2 powders with high γ_{SV}. When the sintering temperature was above 2300 °C, B_4C containing liquid phases appeared which effectively decreased the HfB_2–HfB_2 grain boundary energy by forming a thin layer of B–C film.
2. The microstructure and the mechanical properties of HfB_2. The Young's modulus, hardness and the strength of the as-sintered HfB_2 ceramics did not vary obviously with the sintering temperature when solid state sintering was a dominating sintering mechanism. However, a sharp decrease of mechanical proprieties (except modulus) occurred when liquid phase appeared. HfB_2–2 wt% B_4C sintered at 2150 °C owns the best mechanical properties: Vickers hardness (20.1 GPa), elastic modulus (532 GPa), and flexure strength (492 MPa). These results were comparable with hot pressed HfB_2[3] and higher than ZrB_2 ceramics sintered without external pressure.[8]

Acknowledgements

Financial support from the Chinese Academy of Sciences under the Program for Recruiting Outstanding Overseas Chinese (Hundred Talents Program), the National Natural Science Foundation of China (Nos. 50632070 and 50602048), the International Science and Technology Cooperation Project of Shanghai (No. 08520707800) and the CAS Special Grant for Postgraduate Research, Innovation and Practice are greatly appreciated. The authors thank Dr. Akhilesh Kumar Swarnakar (Department of Metallurgy and Materials Engineering, Katholieke Universiteit Leuven) for the Young's modulus measurement.

References

1. Opeka M, Talmy IG, Wuchina EJ, Zaykoski JA, Causey SJ. Mechanical, thermal and oxidation properties of refractory hafnium and zirconium compounds. *J Eur Ceram Soc* 1999;**19**:2405–14.
2. Fahrenholtz WG, Hilmas GE. Refractory diborides of zirconium and hafnium. *J Am Ceram Soc* 2007;**90**:1347–64.

3. Kalish D, Clougherty EV, Kreder K. Strength, fracture mode, and thermal stress resistance of HfB_2 and ZrB_2. *J Am Ceram Soc* 1969;**52**:30–6.
4. Sciti D, Silvestroni L, Nygren M. Spark plasma sintering of Zr- and Hf-borides with decreasing amounts of $MoSi_2$ as sintering aid. *J Eur Ceram Soc* 2008;**28**:1287–96.
5. Zou J, Zhang G-J, Kan Y-M, Ohji T. Pressureless sintering mechanisms and mechanical properties of hafnium diboride ceramics with pre-sintering heat treatment. *Scr Mater* 2010;**62**:159–62.
6. Sonber JK, Murthy TSRCh, Subramanian C, Kumar S, Fotedar RK, Suri AK. Investigations on synthesis of HfB_2 and development of a new composite with $TiSi_2$. *Int J Refract Met Hard Mater* 2010;**28**: 201–10.
7. Talmy IG, Zaykoski JA, Martin CA. Flexural creep deformation of ZrB_2/SiC ceramics in oxidizing atmosphere. *J Am Ceram Soc* 2008;**91**:1441–7.
8. Fahrenholtz WG, Hilmas GE, Zhang SC, Zhu S. Pressureless sintering of zirconium diboride: particle size and additive effects. *J Am Ceram Soc* 2008;**91**:1398–404.
9. Zhu S, Fahrenholtz WG, Hilmas GE, Zhang SC. Pressureless sintering of carbon-coated zirconium diboride powders. *Mater Sci Eng A* 2007;**459**:167–71.
10. Monteverde F. Hot pressing of hafnium diboride aided by different sinter additives. *J Mater Sci* 2008;**43**:1002–7.
11. Zhang SC, Hilmas GE, Fahrenholtz WG. Pressureless densification of zirconium diboride with boron carbide additions. *J Am Ceram Soc* 2006;**89**:1544–50.
12. Chamberlain AL, Fahrenholtz WG, Hilmas GE. Pressureless sintering of zirconium diboride. *J Am Ceram Soc* 2006;**89**:450–6.
13. Zou J, Zhang G-J, Kan Y-M. Formation of tough interlocking microstructure in ZrB_2–SiC-based ultrahigh-temperature ceramics by pressureless sintering. *J Mater Res* 2009;**24**:2428–34.
14. Zou J, Zhang G-J, Kan Y-M, Wang P-L. Pressureless densification of ZrB_2–SiC composites with vanadium carbide. *Scr Mater* 2008;**59**: 309–12.
15. Zou J, Zhang G-J, Kan Y-M, Wang P-L. Hot-pressed ZrB_2–SiC ceramics with VC addition: chemical reactions, microstructures, and mechanical properties. *J Am Ceram Soc* 2009;**92**:2838–46.
16. Zhu S, Fahrenholtz WG, Hilmas GE, Zhang SC. Pressureless sintering of zirconium diboride using boron carbide and carbon additions. *J Am Ceram Soc* 2007;**90**:3660–3.
17. Baik S, Becher PF. Effect of oxygen contamination on densification of TiB_2. *J Am Ceram Soc* 1987;**70**:527–30.
18. Mishra SK, Das SK, Ray AK, Ramachandrarao P. Effect of Fe and Cr addition on the sintering behavior of ZrB_2 produced by self-propagating high-temperature synthesis. *J Am Ceram Soc* 2002;**85**:2846–8.
19. Monteverde F, Bellosi A, Guicciardi S. Processing and properties of zirconium diboride-based composites. *J Eur Ceram Soc* 2002;**22**:279–88.
20. Silvestroni L, Sciti D. Effects of $MoSi_2$ additions on the properties of Hf- and ZrB_2 composites produced by pressureless sintering. *Scr Mater* 2007;**57**:16–8.
21. Mizuguchi T, Guo S-Q, Kagawa Y. Transmission electron microscopy characterization of hot-pressed ZrB_2 with $MoSi_2$ additive. *J Am Ceram Soc* 2009;**92**:145–8.
22. Rudy E, Windisch S. Part II. Ternary systems. Volume XIII. Phase diagrams of the systems Ti–B–C, Zr–B–C, and Hf–B–C. Ternary phase equilibria in transition metal–boron–carbon–silicon systems. Report No. AFML-TR-65-2. Contract No. USAF 33(615)-1249. Ohio: Air Force Materials Laboratory; Wright-Patterson Air Force Base; 1966. p. 183–8.
23. Ni DW, Zhang GJ, Kan YM, Wang PL. Synthesis of monodispersed fine hafnium diboride powders using carbo/borothermal reduction of hafnium dioxide. *J Am Ceram Soc* 2008;**91**:2709–12.
24. Speyer RF, Lee H. Advances in pressureless densification of boron carbide. *J Mater Sci* 2004;**39**:6017–21.
25. Zhu SM, Fahrenholtz WG, Hilmas GE. Microwave sintering of a ZrB_2–B_4C particulate ceramic composite. *Composites A* 2008;**39**:449–53.
26. Selsing J. Internal stresses in ceramics. *J Am Ceram Soc* 1961;**44**:419–1419.
27. Kang SJL. *Sintering: densification, grain growth and microstructure*. Oxford: Elsevier Butterworth-Heinemann; 2005.